摩擦学学报
TRIBOLOGY

偏压对高功率脉冲磁控溅射法沉积MoN涂层结构及性能的影响

康建，隋旭东，杨淑燕，周海斌，郝俊英，万勇，刘维民

Effect of Bias Voltages on the Structure and Properties of MoN Coatings Deposited by High Power Pulsed Magnetron Sputtering

KANG Jian, SUI Xudong, YANG Shuyan, ZHOU Haibin, HAO Junying, WAN Yong, LIU Weimin

在线阅读 View online: https://doi.org/10.16078/j.tribology.2022198

DOI: 10.16078/j.tribology.2022198

偏压对高功率脉冲磁控溅射法沉积MoN涂层结构及性能的影响

康 建[1,2], 隋旭东[2,3*], 杨淑燕[1,2], 周海斌[2,3], 郝俊英[2,3], 万 勇[1,2*], 刘维民[2]

(1. 青岛理工大学 机械与汽车工程学院, 山东 青岛 266033;
2. 中国科学院兰州化学物理研究所 固体润滑国家重点实验室, 甘肃 兰州 730000;
3. 青岛市资源化学与新材料研究中心, 山东 青岛 266000)

摘 要: 采用高功率脉冲磁控溅射(HiPIMS)方法在9Cr18钢基材上制备了MoN涂层. 系统研究了不同偏压对其结构、力学性能以及摩擦学性能的影响，并优化出耐磨性优异的MoN涂层. 采用场发射扫描电镜分析涂层的表面和截面形貌，采用X-射线衍射仪分析涂层的晶相结构，采用纳米压痕仪测量涂层的硬度和弹性模量，采用摩擦磨损试验机(CSM)评价涂层的摩擦磨损性能. 结果表明：随着偏压的增加，涂层由柱状晶体结构向致密无特征晶体结构转变，相结构以面心立方Mo_2N相为主. HiPIMS方法制备的MoN涂层均表现出较高的硬度(28 GPa以上)和较好的膜基结合力(60 N左右). 摩擦学性能方面，在120 V偏压下沉积得到的涂层摩擦系数最低，为0.24；而在160 V偏压下沉积的涂层磨损率最低，为1.4×10^{-8} $mm^3/(N\cdot m)$.

关键词: HiPIMS; MoN涂层; 偏压; 摩擦磨损; 耐磨性
中图分类号: TH117.1 **文献标志码:** A **文章编号:** 1004-0595(2023)10–1118–10

Effect of Bias Voltages on the Structure and Properties of MoN Coatings Deposited by High Power Pulsed Magnetron Sputtering

KANG Jian[1,2], SUI Xudong[2,3*], YANG Shuyan[1,2], ZHOU Haibin[2,3],
HAO Junying[2,3], WAN Yong[1,2*], LIU Weimin[2]

(*1. School of Mechanical and Automotive Engineering, Qingdao University of Technology, Shandong Qingdao 266033, China*
2. State Key Laboratory of Solid Lubrication, Lanzhou Institute of Chemical Physics, Chinese Academy of Sciences, Gansu Lanzhou 730000, China
3. Qingdao Center of Resource Chemistry and New Materials, Shandong Qingdao 266000, China)

Abstract: In this study, MoN coating was deposited on 9Cr18 steel substrate and Si wafer by high power pulsed magnetron sputtering. The effects of different bias voltages on the microstructure, mechanical properties and tribological properties of MoN coatings were systematically studied, and the coatings with excellent wear resistance were selected. The surface and cross-section morphology of the coating were analyzed by field emission scanning electron microscopy.

Received 23 September 2022, revised 27 December 2022, accepted 27 December 2022, available online 29 December 2022.
*Corresponding author. E-mail: suixudong@licp.cas.cn, Tel: +86-18041376636; E-mail: ywan2007@163.com, Tel: +86-15315328302.
This project was supported by the National Natural Science Foundation of China (51835012, 51975554), the Natural Science Foundation of Gansu Province (21JR7RA081), the Basic Research Projects (2020-JCJQ-ZD-155-12) and CAS "Light of West China".
国家自然科学基金(51835012, 51975554)、甘肃省科技计划(21JR7RA081)、基础研究计划(2020-JCJQ-ZD-155-12)和西部之光项目资助.

The crystal phase structure of the coatings were analyzed by X-ray diffractometer. The hardness and elastic modulus of the coating were measured by nanoindenter. The adhesion of coating was analyzed by scratch tester. Three-dimensional profilometer was used to analyze the wear depth of MoN coating. The friction and wear properties of the coatings were evaluated by CSM friction and wear tester. The results showed that: in terms of microstructure, the surface of MoN coating deposited by HiPIMS technology was compact and smooth, and there were no obvious defects such as large particles and microcracks. With the increase of bias voltage, the ion bombardment on the substrate was enhanced, which made the grown columnar crystal interrupted, the coating changed from columnar crystal structure to compact and featureless crystal structure. And the phase structure was dominated by face-centered cubic Mo_2N phase, with a small amount of Mo phase structure. In terms of mechanical properties, with the increase of bias voltage, the ion bombardment effect increased, and the hardness of the coating gradually increased. When the bias voltage was 160 V, the hardness of the coating was the highest, reaching 33 GPa. The elastic modulus of MoN coating showed a trend of increasing at first and then decreasing, when the bias voltage was 120 V, the maximum elastic modulus was 357.7 GPa. The corresponding increase of H/E and H^3/E^2 values also represented the enhancement of wear resistance of MoN coating. MoN coating deposited by HiPIMS method all showed good coating-substrate adhesion (about 60 N). However, with the increase of bias voltage, the residual stress of MoN coating increased, and when the bias voltage was 160 V, the bonding force decreased to about 58 N. In terms of tribological properties, there was no obvious difference in friction coefficient of MoN coating deposited under different bias voltages, and the average friction coefficient of coating deposited under 120 V bias voltage was the lowest, which was 0.24. In terms of wear rate, the wear rate of S120 and S160 samples was two orders of magnitude lower than that of S40 and S80 samples. This was because the energy bombardment carried by plasma was weak under low bias voltage, the coating deposited on the substrate had low bonding strength and poor compactness. Moreover, the columnar loose structure of MoN coating leads to its low hardness, poor crack propagation resistance and wear resistance, and it was easier to produce microcracks and local spalling during friction. By adjusting and increasing the appropriate bias voltage, the coating structure was denser, and the coating had no crack defects. Meanwhile, with the enhancement of ion bombardment effect, the bonding force and hardness of the coating were increased. The anti-plastic deformation ability of the coating was enhanced, which effectively inhibited the generation and expansion of cracks, and the abrasive particles peeled off during friction were correspondingly reduced. The wear marks of the coating were relatively narrow and shallow, among them, the lowest wear rate of S160 was 1.4×10^{-8} $mm^3/(N\cdot m)$.

Key words: HiPIMS; MoN coating; bias voltage; friction and wear; wear resistance

在航空航天领域，材料的摩擦磨损对航空发动机零部件的使用寿命有显著影响，如主轴轴承磨损失效问题，涡轮叶片叶冠接触面的磨损问题[1-2]. 这不仅对材料的综合性能提出了更严格的要求，而且在某些情况下超出了基材所能达到的性能范围. 为了提升机械零部件的耐磨性、可靠性以及抗疲劳性，采用先进的表面涂层制备技术，结合实际工况下的性能要求，在基材表面制备具有高耐磨性和良好附着性能的涂层，已成为提高零部件使用寿命的有效措施之一[3-4].

目前，航空发动机运动部件涂层制备工艺主要包括热喷涂、电镀、电弧离子镀以及磁控溅射等技术[5-7]. 其中，磁控溅射法制备的涂层因结构致密，表面光滑无大颗粒而被广泛用于运动部件表面耐磨防护[8]. 近年来，科研人员在普通磁控溅射基础上发展了新型高功率脉冲磁控溅射技术(HiPIMS). 相比于直流磁控溅射(DCMS)与电弧离子镀(AIP)，HiPIMS通过在1个脉冲周期内的极短时间施加非常高的脉冲峰值功率密度来实现更高的金属离化率，沉积离子的轰击和蚀刻效应显著增强，参与成膜离子的能量和密度更高[9-10]. 因此，采用该方法制备的涂层膜基结合强度更高，更加光滑致密，缺陷以及金属大颗粒更少. Roychowdhury等[11]通过2种方法将铜和钨溅射到硅片上，结果表明HiPIMS比DCMS方法得到的涂层表面更致密且氧化现象更少. 刘等[12]通过对比HiPIMS和AIP这2种制备方法，证明了AIP制备的涂层表面有着更多的生长缺陷，而HiPIMS制备涂层的表面质量和完整性更好.

MoN涂层具有高硬度、高耐磨性，在宽温域内具有良好的摩擦学性能，是航天高温润滑材料的良好选择之一[13]. Suszko等[14]报道了MoN涂层可以在高温下氧化为具有剪切滑移相的MoO_3，从而达到减摩作用. 由于氮气流量、偏压等沉积参数对涂层结构和性能的影响至关重要. 前期，科研人员主要对此展开了研究工作，徐等[15]采用DCMS制备了不同偏压的MoN涂层，结果表明在-500 V偏压下制备的涂层耐磨性更

好；Wang等[16]研究表明，随氮气流量的增加，MoN涂层由BCC α-Mo相转变为纯FCC Mo_2N相，相结构的转变影响了涂层的结构与性能. 然而，有关于HiPIMS技术制备MoN涂层的研究相对较少. 因此，本文作者采用HiPIMS方法制备了不同偏压下的MoN涂层，并系统研究了偏压对涂层结构、力学性能以及摩擦学性能的影响.

1 试验部分

1.1 涂层制备

采用高功率脉冲磁控溅射方法(HiPIMS)在9Cr18钢($Ra \leqslant 0.5$ μm, HRC50-HRC60)和Si (100)晶片上沉积MoN涂层. 设备配备了德国Huettinger公司生产的新一代大功率脉冲电源(TruPlasma HiPIMS 4000 G2). 靶材选用合琦靶材科技公司生产的纯钼靶材(原子分数99.99%). 首先，将基体分别用石油醚和酒精超声处理10 min，然后将基体用纯氩气干燥并放入真空腔室内. 在开始沉积之前，将腔体真空抽至约3×10^{-3} Pa的基础压力. 同时，为了活化基体，提升膜层附着力，将腔室温度加热至350 ℃. 此外，为了去除基体表面的氧化物层和其他吸附的杂质，所有基体都用Ar离子蚀刻20 min (氩气流量：150 sccm，偏置电压：−850 V). 之后，将转速设置为30 Hz，引入60 sccm氩气，沉积纯钼中间层10 min，以提高涂层与基材的结合性能. 然后，引入15 sccm氮气，并通过控制偏压为40、80、120和160 V来沉积MoN涂层2 h. 为便于后续讨论，在不同偏压下制备的样品分别命名为 S40、S80、S120和S160. 设备示意图如图1所示，详细的沉积参数列于表1中.

1.2 涂层结构与力学性能表征

采用高分辨X射线衍射仪(GIXRD，德国BRUKER公司，D8 ADVANCE)在掠入射模式下(入射角为1°)，分析了不同偏压下沉积MoN涂层的晶相结构. 使用场发射扫描电子显微镜(SEM，日本电子公司, JSM-7610F)观察涂层的表面和横截面形貌. 并使用该设备配备的能量色散光谱仪(EDS，日本电子公司，OXFORD)分析涂层磨痕处的微量元素种类. 为了分析涂层的膜基结合力，使用划痕测试仪(兰州华汇仪器科技公司，MFT-4000)进行划痕试验，加载速度选择100 N/min，终端载荷选择100 N，划动长度为5 mm. 采用纳米压痕仪(奥地利，Anton Paar公司，STEP E400)测试涂层的弹性模量和硬度. 为了排除基材的影响，下压深度选择涂层总厚度的1/10，并对每个样品进行5次压痕测试，并计算相应的平均值和标准差.

1.3 涂层摩擦磨损性能表征

为了评价通过HiPIMS方法制备不同偏压下MoN涂层的摩擦学性能，采用摩擦磨损试验机(CSM，奥地利Anton Paar公司，TRB^3)进行摩擦试验. 具体试验条件如下：空气(温度：25 ℃，相对湿度：40%)，外加载荷

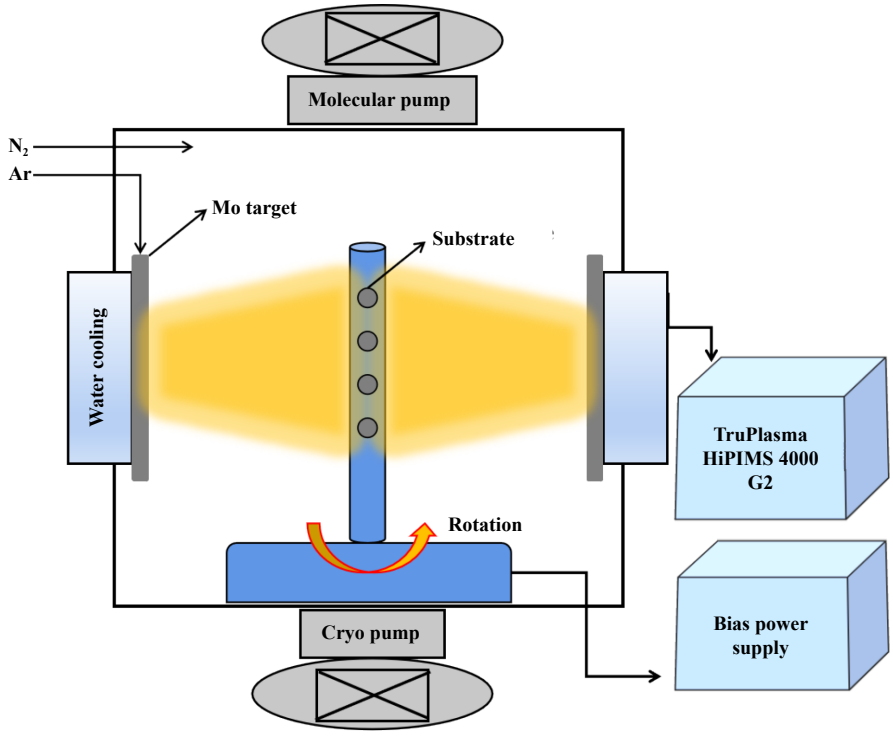

Fig. 1 Schematic diagram of high power pulsed magnetron sputtering (HiPIMS) deposition system

图 1 高功率脉冲磁控溅射(HiPIMS)沉积系统示意图

表 1　通过HiPIMS制备MoN涂层的沉积参数
Table 1　Deposition parameters of MoN coatings deposited by HiPIMS

Parameters	Specification
Working pressure/Pa	0.33
Bias voltage/V	40/80/120/160
Sputtering power/kW	5.5
Peak current/A	280
Frequency/Hz	100
Pulse width/μs	300
Duty cycle	3%

5 N，1次滑动行程为6 mm，总滑动行程为216 m，滑动速度5 Hz. 摩擦副材料选用直径为6 mm的Al_2O_3球. 摩擦试验的总测试时间为1 h. 摩擦试验结束后，通过三维轮廓仪(美国Rtec公司，Rtec3041)观察涂层的磨损轨迹，并计算磨损率. 磨损率由以下公式计算[17]：

$$w = \frac{V}{NS} \tag{1}$$

其中，V是磨损量，单位mm^3，N是载荷，单位N，S是滑动的总路程，单位m.

2　结果与讨论

2.1　MoN涂层的晶体结构

图2给出了采用HiPIMS技术沉积不同偏压下MoN涂层的XRD图谱. 由图2可以看出，排除基材的影响后，所有涂层均表现出5个有效衍射峰. 其中衍射峰角度在40.28°处的微弱衍射峰对应体心立方Mo相(JCPDF42-1120)的(110)晶面，这表示涂层存在少量金属Mo相结构. 在37.5°、43.2°、62.9°和75.5°处的衍射峰，分别对应于面心立方Mo_2N相(JCPDF 25-1366)的

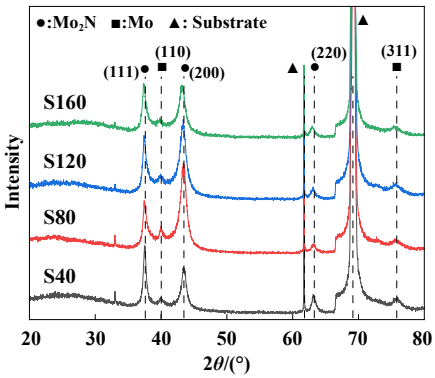

Fig. 2　XRD patterns of MoN coatings deposited under different bias voltages conditions

图 2　不同偏压条件下沉积的MoN涂层的XRD图谱

(111)、(200)、(220)和(311)晶面，这表示涂层主要以面心立方Mo_2N相结构存在[16]. 在偏压从40 V增加到80 V时，涂层的择优取向从(111)晶面转变为(200)，随着偏压继续增加至160 V，涂层的(200)峰位强度有所减弱，择优取向效应不明显. 另外，随偏压的增加，涂层的(111)、(200)以及(311)衍射峰位置有向较低角度偏移的趋势，这是因为轰击离子能量随着偏压的增加而增大，从而导致了涂层晶格参数的增大[18].

2.2　涂层表面与截面形貌

图3所示为不同偏压下制备MoN涂层的表面以及截面的SEM照片. 由图3可以看到，涂层的表面形态成团簇状，没有明显的大颗粒以及缺陷的产生. 而随着偏压的增加，离子轰击涂层表面的能量也逐渐增加，高能离子在一定程度上使涂层的表面更加光滑平整. 由图3(e~f)可以看出，涂层的厚度在855~962 nm. S40的截面形貌呈现1个明显的柱状晶体结构，而随偏压

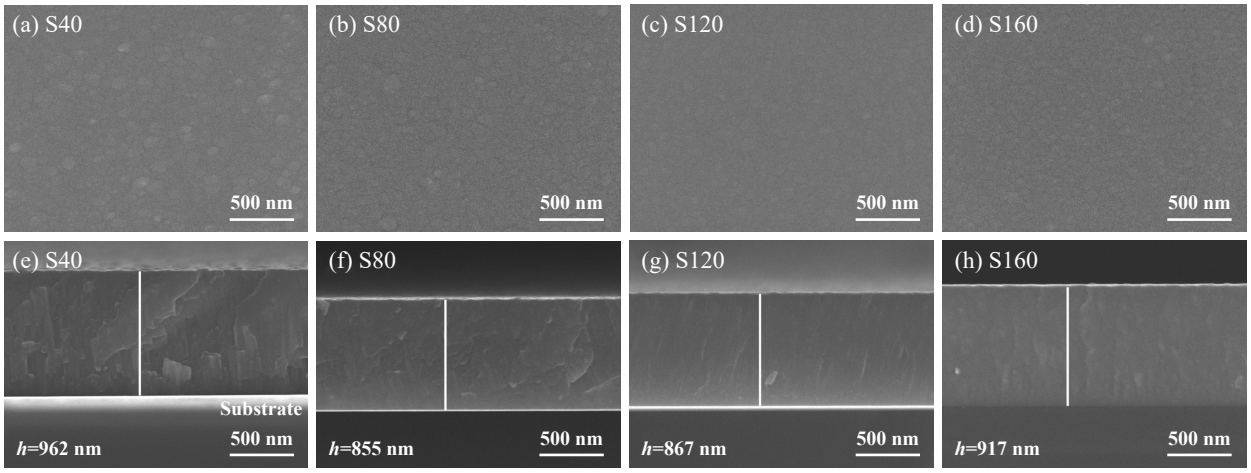

Fig. 3　(a, b, c, d) SEM micrographs of the surface and (e, f, g, h) cross-section of MoN coatings deposited under different bias voltage conditions

图 3　不同偏压条件下沉积的MoN涂层的(a, b, c, d)表面以及(e, f, g, h)截面形貌的SEM照片

增加，离子轰击涂层能量也相应地增强，这增加了其缺陷和成核位点的数量，从而抑制了晶粒的生长，涂层柱状晶体结构逐渐转变为更为致密的结构[19]. 因此，MoN涂层表面的粗糙度与截面结构都与到达涂层表面的轰击能量有关. 而HiPIMS技术本身可以在短脉冲时间内获得电离程度和密度更高的等离子体，又在负偏压的作用下轰击基体，这使所沉积的涂层更加均匀致密. 但如图4所示，由于过高的偏压对硅片的轰击能量更高，应力加剧，这种相互作用造成了涂层在硅片上出现剥落现象. 此外，由于9Cr18钢块和Si片2种基材的热膨胀系数不同，在涂层冷却过程中，二者的收缩程度有很大差异，这导致在2种基材上所产生的残余热应力不同. 从而产生钢块上涂层完好，而硅片上涂层剥落的现象.

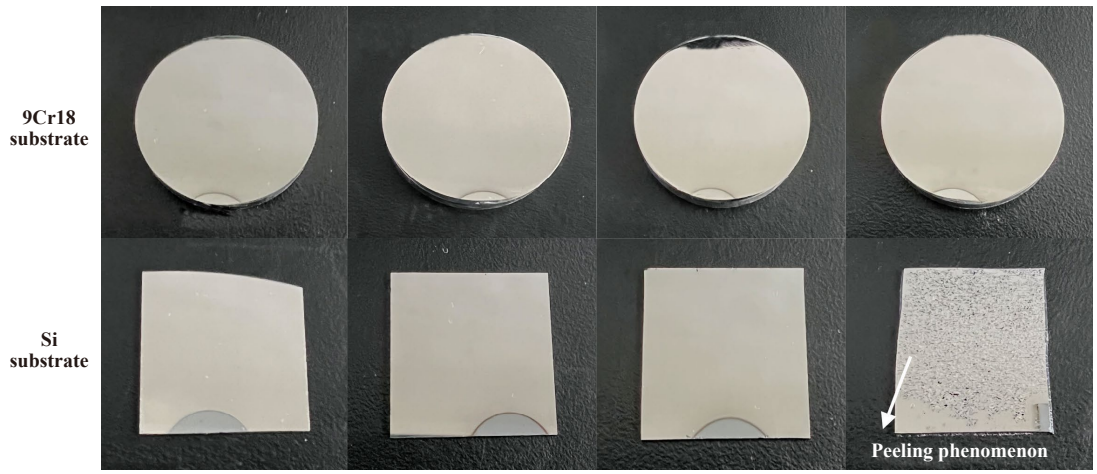

(a) S40 (b) S80 (c) S120 (d) S160

Fig. 4 Image of MoN coating deposited on the surface of 9Cr18 steel and silicon wafer

图 4 在9Cr18钢块与硅片表面沉积MoN涂层的图像

2.3 涂层的硬度

图5(a)所示为不同偏压下沉积的MoN涂层的硬度(H)和弹性模量(E)，如图5(a)所示，随着偏压的增加，涂层的硬度呈略微增加的趋势，由28.5 GPa增加到33.1 GPa. 而涂层的弹性模量先增大后减小，S120样品有着最高的弹性模量，其值为357.7 GPa. 随着偏压的增大，等离子体密度更高，携带的能量更多，从而到达涂层表面的轰击能量更大，涂层的晶粒细化以及致密性得到提升，这使得涂层的硬度提高. H/E与H^3/E^2在一定程度上可以体现涂层的耐磨性以及抗塑性变形能力[20]. 由图5(b)可以看到随着偏压的增加，H/E和H^3/E^2有逐渐增加的趋势，这证明涂层的耐磨性和抗塑性变形能力得到提升.

2.4 涂层的结合力

图6所示为在不同偏压条件下沉积的MoN涂层的摩擦系数和摩擦力曲线与加载力的关系. 在线性增加的载荷作用下进行划痕试验时，当压头划针将涂层划破或出现裂纹时，摩擦力和摩擦系数曲线斜率的突然

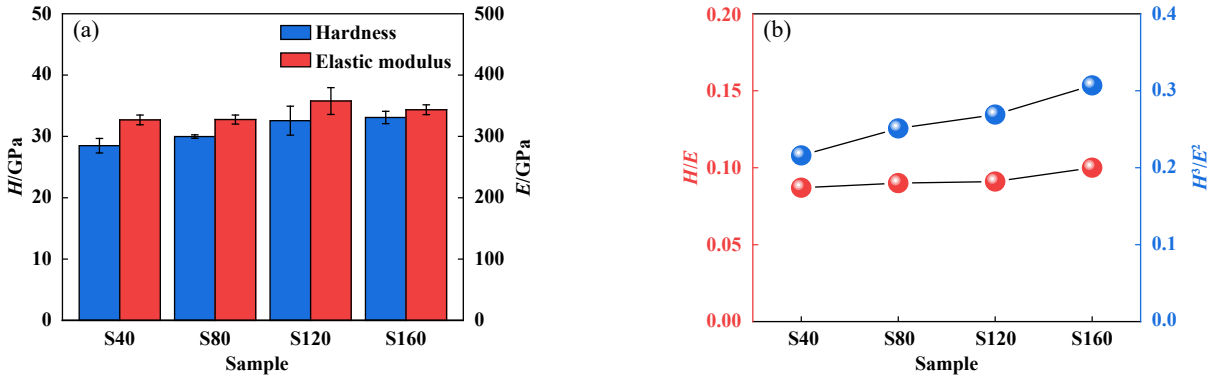

Fig. 5 Hardness and elastic modulus of MoN coatings deposited under different bias voltages conditions: (a) hardness; (b) elastic modulus

图 5 不同偏压条件下沉积的MoN涂层的硬度及弹性模量: (a)硬度; (b)硬度弹性模量

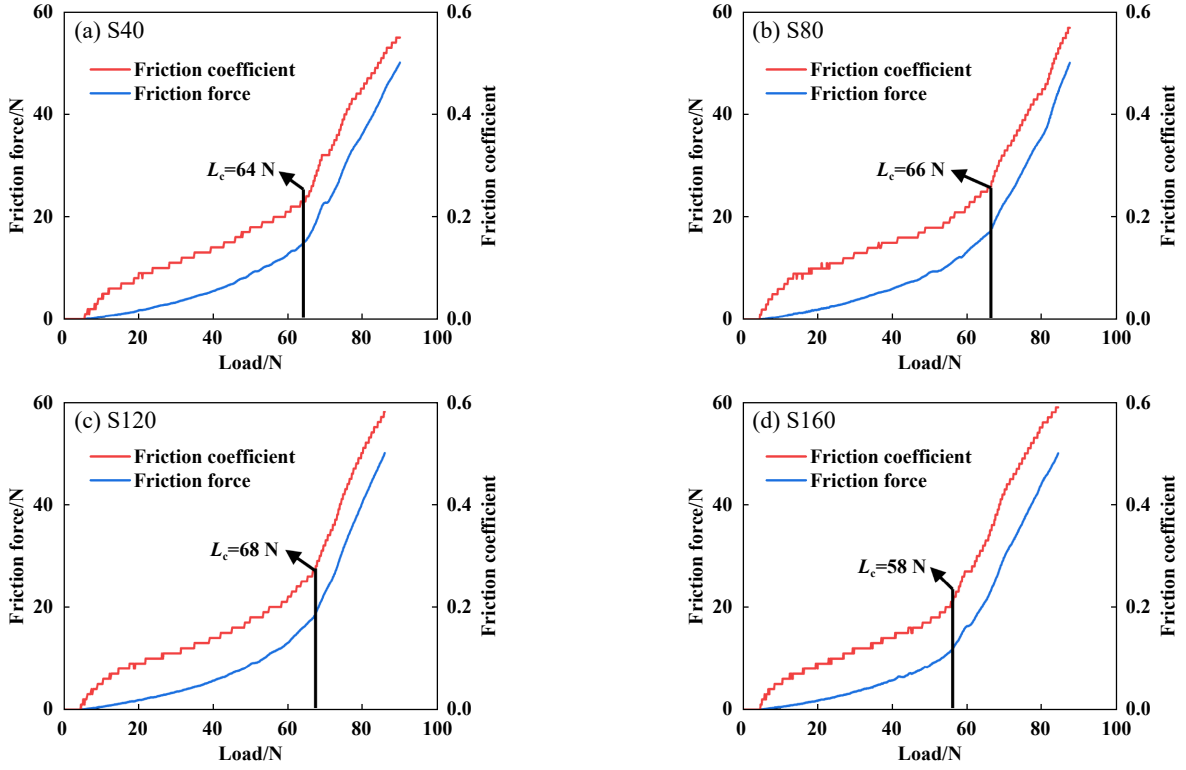

Fig. 6　Image of relationship between friction coefficient curve, friction curve and loading force of MoN coatings deposited under different bias voltages conditions

图 6　在不同偏压条件下沉积的MoN涂层的摩擦系数和摩擦力曲线与加载力的关系图

变化被用作评估涂层临界载荷的标准，相应的临界载荷值(L_C)则作为涂层的结合强度[21-22]. 由图6(a~d)可以看出，不同偏压下的MoN涂层的结合力差距不大，都在60 N左右. 随着偏压的增加，结合力有先增大后减小的趋势. 这可能与偏压进一步增大，涂层内应力相应升高有关，即使如此，S160的L_c值仍为58 N. 综上所述，通过HiPIMS制备的不同偏压下的MoN涂层都有着较优的膜基结合力.

2.5　涂层的摩擦磨损性能

图7所示为不同偏压条件下沉积的MoN涂层的摩擦系数曲线、平均摩擦系数和磨损率. 图7(a)所示为MoN涂层的动态摩擦系数曲线，由图7可知，S40样品在稳定摩擦50 min后，摩擦系数突然增加并且波动剧烈，此时我们判断涂层已经失效. 而由图7(b)可知，S80和S120样品虽然平均摩擦系数较低，分别为0.30和0.24，但在摩擦过程中系数波动较大，这可能与摩擦过程中磨粒剥落有关. 剥落的磨料颗粒继续参与摩擦过程，导致摩擦系数随时间出现较大波动. S160样品的摩擦系数全程最稳定，平均为0.3左右.

图7(c)所示为MoN涂层的磨损率，由图7可以明显看到，偏压对MoN涂层的耐磨性有显著影响. 随着偏压的增加，涂层的耐磨性显著提高. 值得注意的是，S40

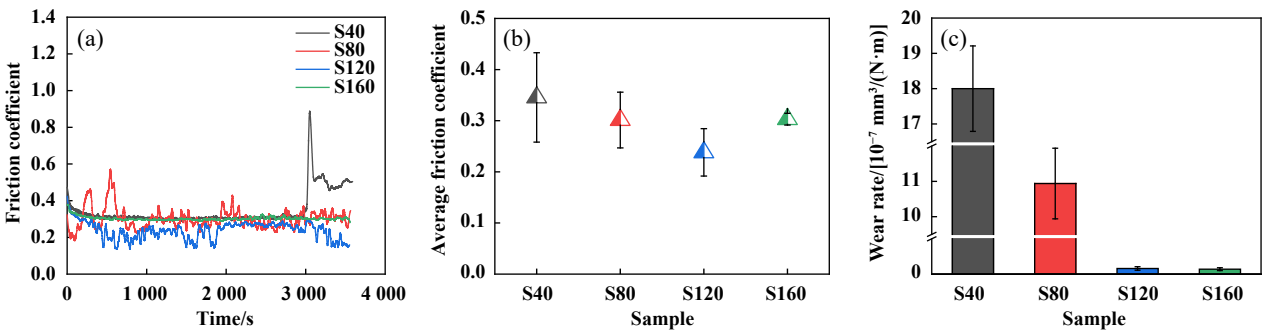

Fig. 7　(a) Friction coefficient curves, (b) average friction coefficient and (c) wear rates of the MoN coatings deposited under different bias voltage conditions

图 7　不同偏压条件下沉积的MoN涂层的(a)摩擦系数曲线(b)平均摩擦系数和(c)磨损率

和S80样品与S120和S160样品的磨损率相差2个数量级. 其中S40样品的磨损率最高，为1.8×10^{-6} mm^3/(N·m)，S120和S160样品的磨损率较低，为1.6×10^{-8}和1.4×10^{-8} mm^3/(N·m). 综上，S40具有最差的耐磨性，S160具有最为优异的耐磨性. 随着偏压的增加，MoN涂层耐磨性更好，这可能归因于高偏压下制备出的样品具有更致密的结构. 同时，为了更好地体现本工作中所沉积的MoN涂层的优异耐磨性，我们将得到的MoN涂层最优磨损率与其他研究人员所制备的不同MoN基涂层的磨损率进行对比[23-27]. 如图8所示，与其他MoN基涂层磨损率对比之下，本工作所沉积的MoN涂层的磨损率最低，表明该涂层耐磨性优异.

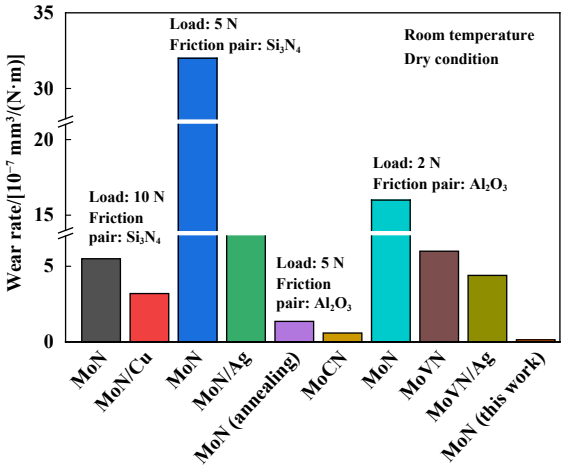

Fig. 8 Comparison of wear rates of MoN coatings deposited by HiPIMS method with coatings deposited by other researchers

图 8 采用HiPIMS法沉积的MoN涂层与其他研究人员沉积的涂层的磨损率比较

图9所示为不同偏压条件下制备的MoN涂层的磨痕及其局部放大位置形貌的SEM照片. 磨痕轨迹也明显对应了MoN涂层磨损率的变化，如图9(a)所示，由于在摩擦过程中，剥落的磨屑磨粒继续参与摩擦行为，在负载的作用下，较硬氧化铝球的刮擦效应对涂层造成严重的磨损，使得磨痕处形成凹槽缺陷. 并且可以在磨痕处观察到少量黑色黏着层，这是由于在摩擦后期涂层剥落后，摩擦磨损直接作用在钢基体上，导致少量磨屑堆积，出现了黏附层. 观察S80样品磨痕的SEM照片可以发现，首先是磨痕宽度的减小，由507 μm减小至439 μm，其次是失效部位出现在摩擦副与涂层接触应力最集中的部位. 这说明随着偏压的增加，MoN涂层变得更加耐磨. 在负载的作用下，摩擦磨损首先从接触应力最大的区域开始，随后由于涂层剥落碎片

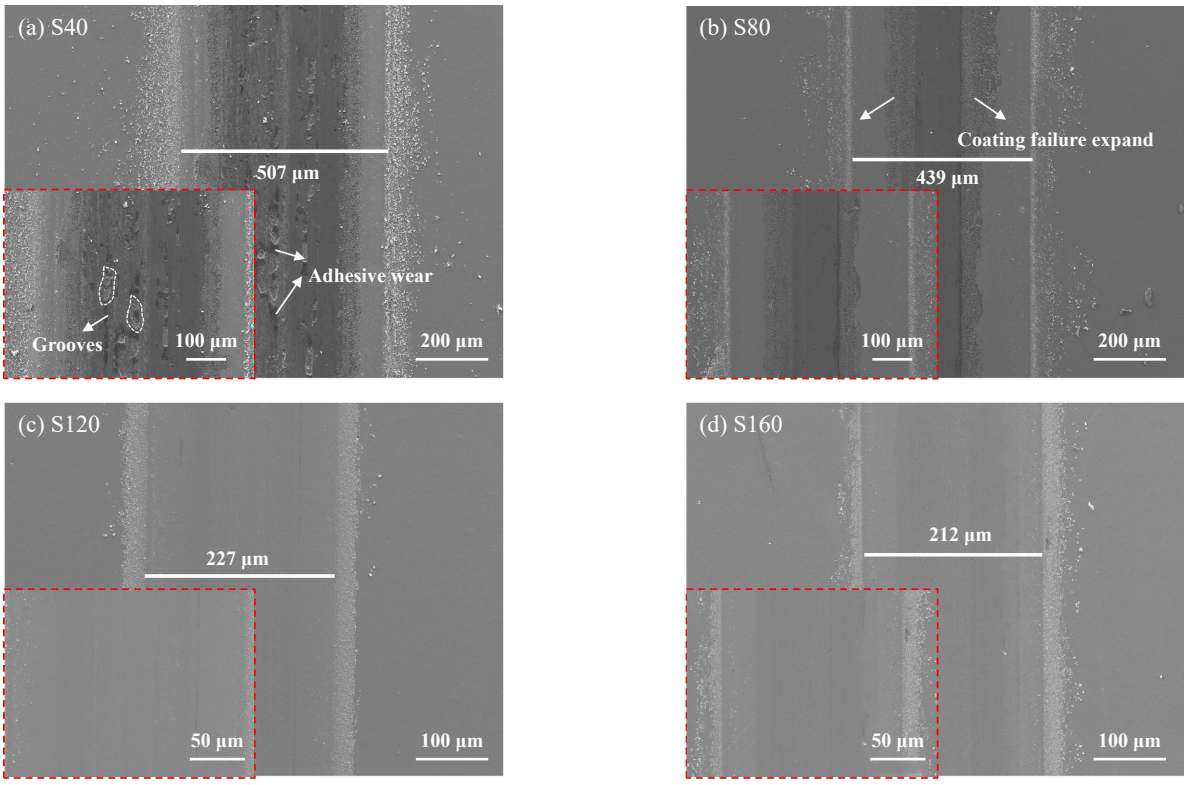

Fig. 9 SEM micrographs of wear scars and their local enlarged morphologies of MoN coatings deposited under different bias voltage conditions

图 9 不同偏压条件下沉积的MoN涂层的磨痕及其局部放大位置形貌的SEM照片

的堆积挤压，又向涂层的两侧释放应力，导致涂层失效部位的扩展. 相较于此，S120和S160样品的磨痕较为光滑平整，磨痕宽度也更小，说明2个样品均只发生了轻微的磨粒磨损. 其中，S160样品具有最小的磨痕宽度，为212 μm. 综上所述，偏压导致涂层耐磨性变化的原因，我们认为在低偏压条件下制备的MoN涂层截面致密性较差、硬度较低，在摩擦过程中容易发生剥落、塑性变形，导致涂层磨损严重. 而在高偏压下制备的MoN涂层截面更致密、硬度更高，抗承载能力和抗塑性变形能力更强.

图10所示为不同偏压条件下制备的MoN涂层的三维磨痕形貌图，由图10可以看出，涂层的磨痕深度和宽度呈逐渐减小的趋势. 但是，由S40和S80样品对比发现，虽然S40样品的深度最深达到2 μm，但更像是刮擦的沟槽所造成的，磨损更多的是向两边扩展. 而S80样品的磨损行为，向下的负载力造成的摩擦磨损行为占据主导，这表明涂层致密性和耐磨性的提升阻止了磨损向两侧扩展的行为. 随着偏压的逐渐增加，S120和S160样品似乎也有这种趋势. 由于S160的耐磨性更好，磨损率最低，同样地S160的磨痕深度也最低，约为110 nm.

2.6　涂层的摩擦磨损机理

图11给出了采用HiPIMS法沉积不同偏压下MoN涂层的摩擦磨损示意图. 如图11所示，在低偏压下，左侧涂层呈疏松柱状结构，使得涂层硬度较低，抵抗裂纹扩展能力以及耐磨性较差. 偏压较小时，等离子体携带的能量轰击作用弱，沉积在基材上的涂层结合强度较低，致密性较低，所以在摩擦过程中更容易出现

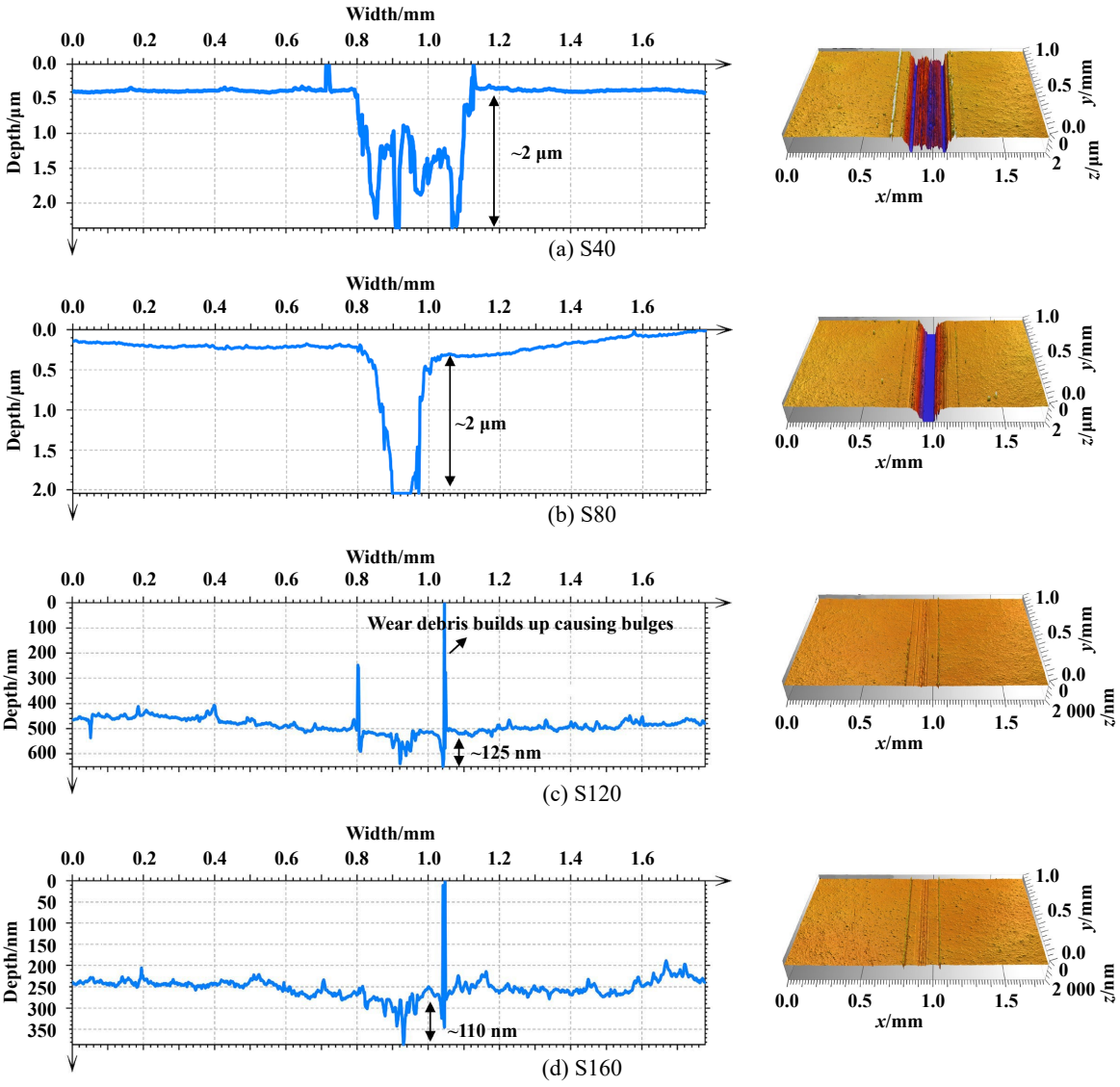

Fig. 10　Three-dimensional wear scar morphologies of MoN coatings prepared under different bias voltage conditions

图 10　不同偏压条件下沉积的MoN涂层的三维磨痕形貌图

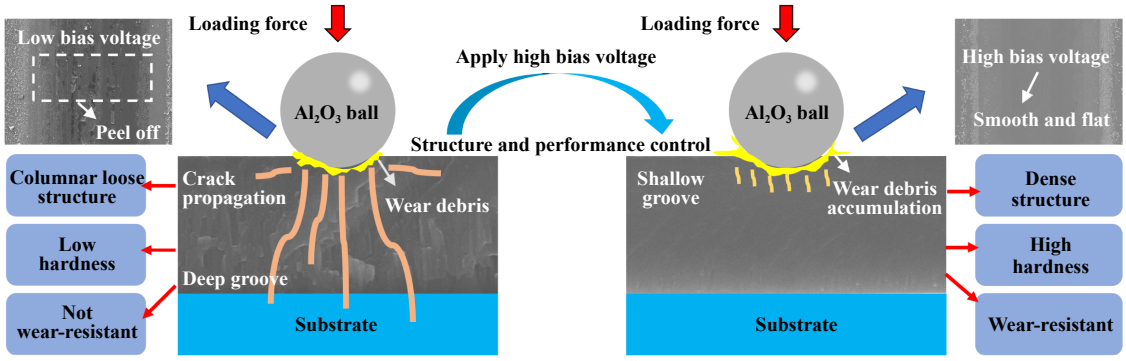

Fig. 11 Schematic diagram of the antiwear and antifriction mechanism of MoN coatings deposited by HiPIMS method under different bias voltages conditions

图 11 采用HiPIMS法在不同偏压条件下沉积的MoN涂层的抗磨减摩机理示意图

微裂纹和局部剥落，剥离的磨粒在负载力作用下造成了深的凹槽和犁沟，同时在往复摩擦过程中受到挤压力的作用向两边扩展，从而造成更严重的磨损. 通过调整增加合适的偏压，可以在右侧获得结构更加致密并且无孔隙缺陷的涂层，膜基结合力也随着离子轰击作用的增大而略有提升，这有效阻止了裂纹扩展. 并且随着偏压的增大，涂层的硬度提高，同时H/E与H^3/E^2升高，因此其抗塑性变形能力有所增强. 硬度和致密度的提高也抑制了裂纹的产生和扩展，同时在摩擦过程中剥落的磨粒也相应减少，涂层磨损痕迹相对较窄且浅，这意味着磨损率更低.

3 结论

采用高功率脉冲磁控溅射技术在9Cr18钢基材与硅片上沉积了MoN涂层，探究了不同偏压对MoN涂层结构、机械性能以及摩擦学性能的影响，得到以下结论：

a. 微观结构方面，随着偏压的增加，涂层表面粗糙度降低，截面由明显的柱状晶体结构转变为更致密的晶体结构. XRD结果表明，所有涂层主要以面心立方Mo_2N相形式存在，偏压对晶相结构的择优取向效应有显著影响.

b. 机械性能方面，随着偏压的增加，硬度逐渐增加，偏压160 V涂层时，硬度最高，达到33 GPa. 此外，所有MoN涂层均有着60 N左右较强的膜基结合强度.

c. 摩擦学性能方面，往复摩擦过程中，偏压为120 V涂层表现出最低的平均摩擦系数(0.24). 而随着偏压进一步增加，结构更致密，硬度更高，耐磨性更好，偏压为160 V涂层表现出最低的磨损率，为1.4×10^{-8} $mm^3/(N\cdot m)$.

参 考 文 献

[1] Chen Chao, Zeng Zhaoyang, Luo Jun, et al. Failure mode analysis of aeroengine spindle bearings[J]. Lubrication Engineering, 2020, 45(3): 126–131 (in Chinese) [陈超, 曾昭洋, 罗军, 等. 航空发动机主轴轴承失效模式分析[J]. 润滑与密封, 2020, 45(3): 126–131]. doi: 10.3969/j.issn:0254-0150.2020.03.022.

[2] Chen Lishun, Wang Yanling, Lu Jianhong, et al. Development of study and application of aeroengine sealing technology[J]. Aeronautical Manufacturing Technology, 2008, 51(8): 82–84,95 (in Chinese) [陈礼顺, 王彦岭, 卢建红, 等. 航空发动机封严技术的研究和应用进展[J]. 航空制造技术, 2008, 51(8): 82–84,95]. doi: 10.16080/j.issn:1671-833x.2008.08.014.

[3] Wo P C, Munroe P R, Jiang Z T, et al. Enhancing toughness of CrN coatings by Ni addition for safety-critical applications[J]. Materials Science and Engineering:A, 2014, 596: 264–274. doi: 10.1016/j.msea.2013.12.064.

[4] Etsion I, Halperin G, Becker E. The effect of various surface treatments on piston pin scuffing resistance[J]. Wear, 2006, 261(7−8): 785–791. doi: 10.1016/j.wear.2006.01.032.

[5] He Jinmei, Cai Qing, Zhang Lujuan. Application and development of surface engineering technology in aero-engine manufacturing[J]. Metal Working (Metal Cutting), 2016(24): I0002–I0002,1,2 (in Chinese) [何金梅, 蔡卿, 张麓娟. 表面工程技术在航空发动机制造中的应用与发展[J]. 金属加工(冷加工), 2016(24): I0002–I0002,1,2].

[6] Hao Bing, Li Chenggang. Application of surface coating technologies to aeroengines[J]. Aeroengine, 2004, 30(4): 38–40 (in Chinese) [郝兵, 李成刚. 表面涂层技术在航空发动机上的应用[J]. 航空发动机, 2004, 30(4): 38–40]. doi: 10.3969/j.issn.1672-3147.2004.04.011.

[7] Sui Yusong, Xu Kejun, Jiang Longping, et al. Ceramic coating of aeroengine turbine blade[J]. Materials Protection, 2001, 34(3): 38–40,0 (in Chinese) [隋育松, 徐可君, 江龙平, 等. 陶瓷涂层在航空发动机涡轮叶片表面处理中的应用[J]. 材料保护, 2001, 34(3): 38–40,0]. doi: 10.16577/j.cnki.42-1215/tb.2001.03.021.

[8] Xiang J Y, Lin Z X, Renoux E, et al. Microstructure evolution and indentation cracking behavior of MoN multilayer films[J]. Surface and Coatings Technology, 2018, 350: 1020–1027. doi: 10.1016/j.

surfcoat.2018.02.074.

[9] Ma D, Harvey T J, Wellman R G, et al. Cavitation erosion performance of CrAlYN/CrN nanoscale multilayer coatings deposited on Ti_6Al_4V by HIPIMS[J]. Journal of Alloys and Compounds, 2019, 788: 719–728. doi: 10.1016/j.jallcom.2019.02.238.

[10] Wu Wanyu, Chan M Y, Hsu Y H, et al. Bioapplication of TiN thin films deposited using high power impulse magnetron sputtering[J]. Surface and Coatings Technology, 2019, 362: 167–175. doi: 10.1016/j.surfcoat.2019.01.106.

[11] Roychowdhury T, Shah D, Jain V, et al. Multi-instrument characterization of HiPIMS and DC magnetron sputtered tungsten and copper films[J]. Surface and Interface Analysis, 2020, 52(7): 433–441. doi: 10.1002/sia.6753.

[12] Liu Yuan, Ding Jicheng, Xu Yuxiang, et al. Preparation and cutting performance of AlTiN coatings by arc ion plating and high power pulsed magnetron sputtering[J]. Surface Technology, 2022, 51(2): 57–65 (in Chinese) [刘源, 丁继成, 许雨翔, 等. 电弧离子镀和高功率脉冲磁控溅射AlTiN涂层及其切削性能研究[J]. 表面技术, 2022, 51(2): 57–65]. doi: 10.16490/j.cnki.issn.1001-3660.2022.02.006.

[13] Gassner G, Mayrhofer P H, Kutschej K, et al. Magnéli phase formation of PVD Mo-N and W-N coatings[J]. Surface and Coatings Technology, 2006, 201(6): 3335–3341. doi: 10.1016/j.surfcoat.2006.07.067.

[14] Suszko T, Gulbiński W, Jagielski J. The role of surface oxidation in friction processes on molybdenum nitride thin films[J]. Surface and Coatings Technology, 2005, 194(2-3): 319–324. doi: 10.1016/j.surfcoat.2004.07.119.

[15] Xu Xing, Su Fenghua, Li Zhujun. Effects of pulse bias on structure and properties of MoN film deposited by DC magnetron sputtering[J]. China Surface Engineering, 2019, 32(2): 54–62 (in Chinese) [徐星, 苏峰华, 李助军. 脉冲偏压对直流磁控溅射沉积MoN薄膜结构及性能的影响[J]. 中国表面工程, 2019, 32(2): 54–62]. doi: 10.11933/j.issn.1007-9289.20181106003.

[16] Wang Tao, Zhang Guojun, Ren Shuai, et al. Effect of nitrogen flow rate on structure and properties of MoN_x coatings deposited by facing target sputtering[J]. Journal of Alloys and Compounds, 2017, 701: 1–8. doi: 10.1016/j.jallcom.2017.01.077.

[17] Patnaik L, Maity S R, Kumar S. Mechanical and tribological assessment of composite AlCrN or a-C: Ag-based thin films for implant application[J]. Ceramics International, 2021, 47(5): 6736–6752. doi: 10.1016/j.ceramint.2020.11.016.

[18] Pogrebnjak A D, Yakushchenko I V, Bagdasaryan A A, et al. Microstructure, physical and chemical properties of nanostructured (Ti-Hf-Zr-V-Nb)N coatings under different deposition conditions[J]. Materials Chemistry and Physics, 2014, 147(3): 1079–1091. doi: 10.1016/j.matchemphys.2014.06.062.

[19] Lu Xiaolong, Zhang Cunxiu, Zhang Xiao, et al. Dependence of mechanical and tribological performance on the microstructure of (CrAlTiNbV)Nx high-entropy nitride coatings in aviation lubricant[J]. Ceramics International, 2021, 47(19): 27342–27350. doi: 10.1016/j.ceramint.2021.06.156.

[20] Ma Hairui, Miao Qiang, Zhang Gaohui, et al. The influence of multilayer structure on mechanical behavior of TiN/TiAlSiN multilayer coating[J]. Ceramics International, 2021, 47(9): 12583–12591. doi: 10.1016/j.ceramint.2021.01.117.

[21] Cheng Kenghao, Weng C H, Lai C H, et al. Study on adhesion and wear resistance of multi-element (AlCrTaTiZr)N coatings[J]. Thin Solid Films, 2009, 517(17): 4989–4993. doi: 10.1016/j.tsf.2009.03.139.

[22] Wang Zeyong, Feng Changjie, Shi Chao, et al. Effect of trace Ag on tribological properties of TiAlN coating[J]. Tribology, 2020, 40(5): 634–646 (in Chinese) [王泽勇, 冯长杰, 师超, 等. 微量Ag 元素对TiAlN 涂层摩擦学性能的影响[J]. 摩擦学学报, 2020, 40(5): 634–646]. doi: 10.16078/j.tribology.2020004.

[23] Xu Xing, Su Fenghua, Li Zhujun. Microstructure and tribological behaviors of MoN-Cu nanocomposite coatings sliding against Si_3N_4 ball under dry and oil-lubricated conditions[J]. Wear, 2019, 434–435: 202994. doi: 10.1016/j.wear.2019.202994.

[24] Xu Xing, Sun Jianfang, Su Fenghua, et al. Microstructure and tribological performance of adaptive MoN-Ag nanocomposite coatings with various Ag contents[J]. Wear, 2022, 488–489: 204170. doi: 10.1016/j.wear.2021.204170.

[25] Qian Jianguo, Li Shuxin, Pu Jibin, et al. Effect of heat treatment on structure and properties of molybdenum nitride and molybdenum carbonitride films prepared by magnetron sputtering[J]. Surface and Coatings Technology, 2019, 374: 725–735. doi: 10.1016/j.surfcoat.2019.06.062.

[26] Wang Wenzhe, Zheng Shaoxian, Pu Jibin, et al. Microstructure, mechanical and tribological properties of Mo-V-N films by reactive magnetron sputtering[J]. Surface and Coatings Technology, 2020, 387: 125532. doi: 10.1016/j.surfcoat.2020.125532.

[27] Wang Wenzhe, Pu Jibin, Cai Zhaobing, et al. Insights into friction properties and mechanism of self-lubricating MoVN-Ag films at high temperature[J]. Vacuum, 2020, 176: 109332. doi: 10.1016/j.vacuum.2020.109332.